Available online at www.sciencedirect.com
ScienceDirect
Thin Solid Films 516 (2008) 6197–6204
www.elsevier.com/locate/tsf

# Deposition of yttrium oxide thin films in supercritical carbon dioxide

Theodosia Gougousi *, Zhiying Chen

*Department of Physics, University of Maryland Baltimore County, Baltimore, Maryland 21250, USA*

Received 11 May 2007; received in revised form 20 November 2007; accepted 21 November 2007
Available online 4 March 2008

**Abstract**

A synthetic avenue for the formation of yttrium oxide thin films on Si native oxide surfaces is demonstrated by the reaction of Tris(2,2,6,6-tetramethyl-3,5-heptanedionato) yttrium(III) with inorganic ($H_2O_2$) and organic (tert-butyl and di-tert-amyl) peroxides in supercritical carbon dioxide. The reactions are carried out in a hot wall reactor at temperatures below 130 °C and pressures ranging from 13.10 to 22.75 MPa. Spectroscopic Ellipsometry verifies thin film formation and X-ray photoelectron spectroscopy and Fourier transform infrared spectroscopy measurements confirm formation of yttrium oxide films and the presence of carbonate and hydroxide species which are removed after high temperature anneals.


*PACS:* 81.10.Dn; 81.05.Je; 81.20.-n
*Keywords:* Yttrium oxide; Supercritical carbon dioxide; Deposition process

## 1. Introduction

Yttrium oxide ($Y_2O_3$) is a very interesting material for electronic and optical applications because of its high refractive index (1.7–1.9) and dielectric constant (10–17), high melting point (~2439 °C), and large optical band gap (~5.5 eV) [1–4]. $Y_2O_3$ is considered as a potential gate dielectric material for the replacement of silicon dioxide in complementary metal oxide semiconductor devices [4,5]. It is also viable as coating or waveguide material in optical devices due to a high melting point and refractive index [1,4,6].

A variety of chemical methods have been used to deposit $Y_2O_3$ films, including chemical vapor deposition (CVD) [7–9], electron-beam evaporation [10], molecular-beam epitaxy [11], and atomic layer deposition [12]. All these methods are vacuum-based techniques that require relatively high substrate temperatures even when used in conjunction with plasma excitation, to assist in the precursor adsorption, oxidation and by-product desorption. For example, Sarma et al. report a substrate temperature of 580 °C for the $Y_2O_3$ CVD from Yttrium di-pivalyol methanate and $O_2$ [7]. Niu et al. report an $Y_2O_3$ Plasma Enhanced Chemical Vapor Deposition (PECVD) process using Tris(2,2,6,6-tetramethyl-3,5-heptanedionato) yttrium(III) ($Y(tmhd)_3$) precursor and $O_2$ plasma activation at 350–450 °C substrate temperature [9]. $Y_2O_3$ thermal ALD has been accomplished at lower temperatures (150–280 °C) using yttrium *tris*-(*N*,*N*′-diisopropylacetamidinate) and water [12]. High temperature processing, may enhance the formation of interfacial layers resulting in significant device performance degradation [4], and is incompatible with deposition on temperature sensitive materials. Physical vapor deposition techniques such as radio-frequency magnetron sputtering [13], and pulsed laser deposition [14] sometimes circumvent the high temperature requirement but because they are line of sight techniques they offer poor step coverage and film conformality.

Supercritical fluids have attracted considerable attention recently in semiconductor manufacturing for processes ranging from wafer cleaning, photoresist-stripping and drying, to the deposition of porous thin films, and metal and metal oxide thin films [15–18]. Of all supercritical fluids, carbon dioxide ($scCO_2$) has attracted the most interest because it has an easily accessible critical point of 7.38 MPa and 31.0 °C [19]. At the critical point, carbon dioxide has a molecular density as high as

* Corresponding author.
*E-mail address:* gougousi@umbc.edu (T. Gougousi).

0040-6090/$ - see front matter © 2007 Elsevier B.V. All rights reserved.
doi:10.1016/j.tsf.2007.11.104

that of liquids, high diffusivity and viscosity comparable to that of gases, zero surface tension, and good solvent capability. Additionally, $scCO_2$ is inexpensive, has low toxicity, it is nonflammable, and environmentally and chemically benign [20]. In this study, we demonstrate a low temperature synthetic route for the formation of yttrium oxide thin films using reactions of inorganic and organic peroxides with metal organic complexes soluble in supercritical carbon dioxide.

## 2. Experimental details

Yttrium oxide thin films are deposited on native oxide Si (100) surfaces in a ~25 ml high-pressure stainless steel cell with sapphire windows purchased from Thar technologies. Fig. 1(a) shows a schematic of the reactor system. $CO_2$ is delivered using an ISCO 260D syringe pump through a high-pressure manifold. Resistive heaters with feedback control are used to keep the temperature of the reaction cell within ± 1 °C of the set point value. Before each experiment, a piece of Si is placed inside the cell along with approximately 20–30 mg of precursor and the cell is flushed with $CO_2$ for 3 min. Then, the cell is sealed, heated to 45 °C for ten minutes and pressurized with $CO_2$ to 8.62 MPa. When the target pressure is reached, the cell is heated to the desired reaction temperature, and the precursor is allowed to dissolve. The oxidizer solutions, (typically 0.2–0.4 ml) are introduced in two different ways: (1) placed in a quartz thimble simultaneously with the precursor; and (2) injected in the deposition cell after the temperature has reached the desired reaction temperature. After a set reaction time, typically 30 min, the cell is purged with $CO_2$ and the effluent is filtered in an activated charcoal bed before venting. Upon removal from the cell, the as-deposited films are cleaned with acetone in a sonic bath for one minute to remove the precipitated reaction byproducts.

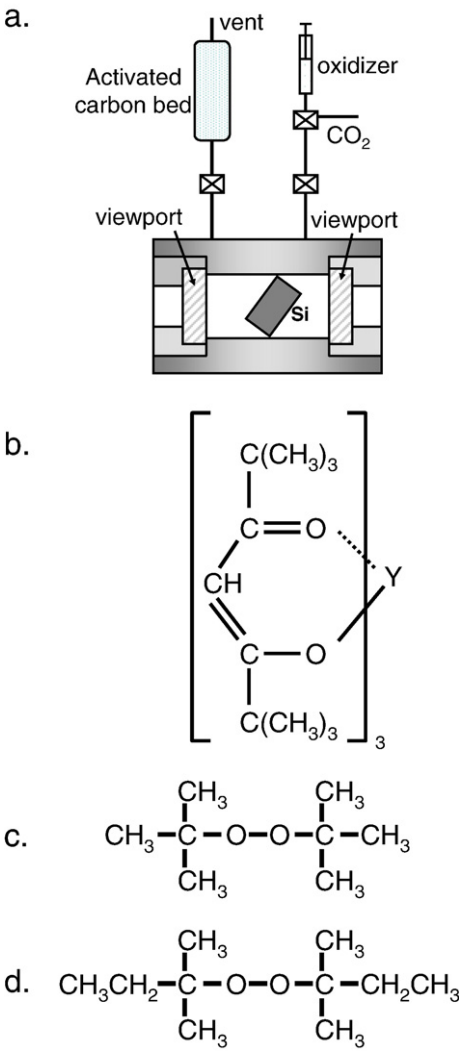


Fig. 1. (a) A schematic of the high pressure cell and associated hardware used for the film deposition. (b) Structure of $Y(tmhd)_3$. (c) Structure of tert-butyl peroxide. (d) Structure of di-tert-amyl peroxide.

Tris(2,2,6,6-tetramethyl-3,5-heptanedionato) yttrium(III), (98+%, 99.9%−Y) ($Y(tmhd)_3$) (Strem Chemicals) that exhibits good solubility in $scCO_2$ is chosen as the metal precursor (Fig. 1(b)) and used as received. The precursor is stored in a well-sealed desiccator to prevent any reaction with ambient moisture. Coleman-grade $CO_2$ with 99.99% purity is used without further purification. The three oxidizers used in this work are: a 30% aqueous solution of hydrogen peroxide (FisherChemical), tert-butyl peroxide ($(CH_3)_3COOC(CH_3)_3$, 98%, Aldrich) (Fig. 1(c)), and di-tert-amyl peroxide ($(C_2H_5C(CH_3)_2OOC(CH_3)_2C_2H_5$, 97%, Aldrich) (Fig. 1(d)).

The sample composition is characterized by X-ray photo-electron spectroscopy (XPS) and transmission Fourier transform infrared spectroscopy (FTIR). The XPS measurements are carried out ex-situ with a Kratos AXIS 165 (Mg X-ray source, 1253.6 eV), equipped with a hemispherical analyzer (165 mm radius). The data were obtained with pass energy of 40 eV at 90° from the sample surface. A survey spectrum with a step size of 0.5 eV is first recorded to identify the surface elements. High-resolution spectra for detailed analysis are recorded with a 0.1 eV step size. All XPS spectra are referenced to the adventitious C 1s peak at a binding energy of 285.0 eV. The samples were not sputter cleaned prior to analysis. A Thermo-Nicolet IR bench is used for both mid- and far-IR spectrum acquisition in the transmission mode with 256 scans at 4 $cm^{-1}$ resolution. The instrument is purged using purified air with low concentrations of moisture and $CO_2$. A background spectrum is collected after each measurement using a substrate fragment that originated from the same wafer as the deposited substrate. All the IR spectra presented in this article were reprocessed using the appropriate background spectrum. The film thickness is measured using a Wollam α-SE fixed-angle (70°) Spectroscopic (300–900 nm) Ellipsometer. The film thickness reported represents the average of several measurements across the sample. The surface morphology of the films is examined using a Thermo Microscopes Autoprobe atomic force microscope (AFM) in the contact mode. Film anneals were performed with a Heatpulse Rapid Thermal Annealer in Ar ambient.

## 3. Results

Formation of yttrium oxide films was achieved at temperatures ranging from 80 to 130 °C and pressure from 13.10 to

22.75 MPa using $Y(tmhd)_3$ as precursor with three different oxidizers: two organic peroxides (tert-butyl and di-tert-amyl proxides) and a 30% aqueous solution of $H_2O_2$. The two organic peroxides were loaded in the cell in a thimble simultaneously with the $Y(tmhd)_3$ precursor while the hydrogen peroxide solution was injected into the cell at the reaction temperature. The hot wall reactor arrangement resulted in deposition on all heated surfaces including the cell view ports and the deposition rate was found to depend on both the process temperature and pressure and in general ranged between 4–10 Å/min. Because of the static arrangement of the cell the deposition rate was not constant throughout the deposition cycle but seemed to decrease with time indicative of the depletion of the reactants.

### 3.1. $Y(tmhd)_3$ and tert-butyl peroxide

Fig. 2(a–c) shows the high-resolution, background corrected XPS spectra for Y 3d (Fig. 2a), C 1s (Fig. 2b), and O 1s (Fig. 2c) core electrons for $Y_2O_3$ films deposited using $Y(tmhd)_3$ and tert-butyl peroxide at 80 °C, 14.48 MPa. The Y 3d spectrum for the as-deposited film in Fig. 2a indicates that the yttrium in the films is oxidized, since a metallic Y 3d peak at 156.0 eV is not observed. In addition, there is no evidence for Y–Si bonds in the Y 3d spectrum, since the binding energy for Y 3d in yttrium silicide is expected to be ~0.2 eV lower than the metallic peak position [21], and additionally the high-resolution scans in the Si 2p range shows no intensity (data not shown). Elemental analysis of the XPS data yields an O to Y ratio higher than the 1.5 expected for stoichiometric $Y_2O_3$ indicating the presence of excess O in the films.

The Y $3d_{5/2}$ and $3d_{3/2}$ peaks for the as-deposited film appear at 158.6 eV and 160.6 eV respectively, exhibiting a positive chemical shift of 1.8 eV from the nominal value of 156.8 and 158.9 eV for the Y $3d_{5/2-3/2}$ doublet in $Y_2O_3$ [22]. Additionally a shoulder is observed at ~164.5 eV. The observed positive chemical shift implies that the Y atoms in the as-deposited film

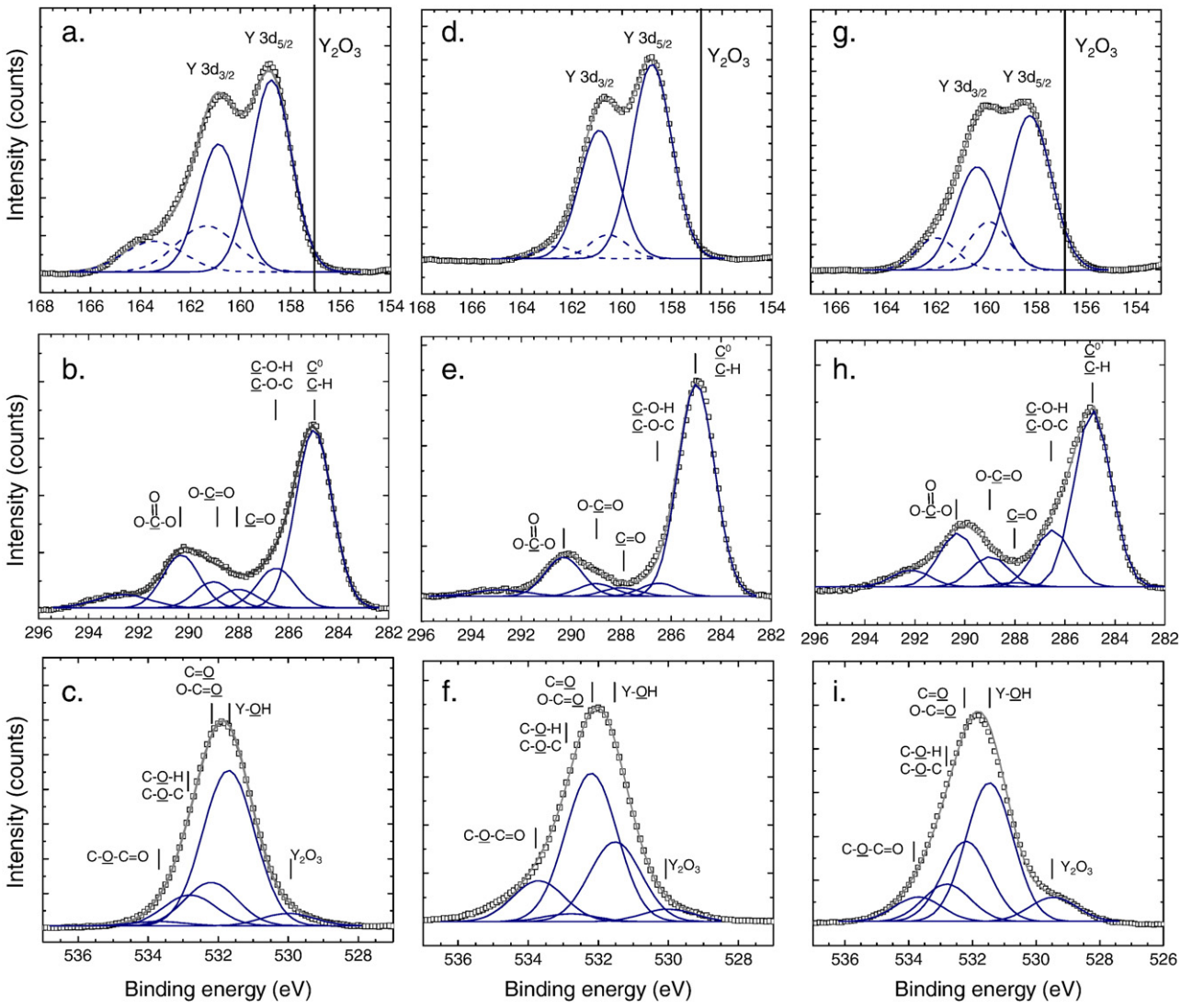


Fig. 2. Y 3d, C1s, and O 1s high-resolution XPS spectra for yttrium oxide films deposited from (a–c) $Y(tmhd)_3$ and tert-butyl peroxide at 80 °C, 14.48 MPa (d–f) $Y(tmhd)_3$ and di-tert-amyl peroxide, 90 °C, 15.86 MPa and (g–i) $Y(tmhd)_3$ and hydrogen peroxide, 130 °C, 22.75 MPa. The solid squares represent the experimental points and the overlaying solid line is the result of Gaussian multipeak fitting.

may be bonded to more electronegative elements. Si mixing in the films in the form of Y–O–Si, may account for the observed shift [23], however, the high-resolution scans in the Si 2p range shows no intensity (data not shown). Y-containing films are known to react with ambient moisture [24], [25] even after film anneals at 900 °C [26] to form hydroxylated Y–OH sites. These sites are susceptible to further reaction with carbon dioxide to form carbon and oxygen containing species such as carbonates and hydroxycarbonates [27–29]. All these species are known to produce positive chemical shifts in the Y binding energy [26,30,31].

The peak height ratio for the Y $3d_{5/2}$ to $3d_{3/2}$ peaks is 1.19, smaller than the theoretically expected ratio of 1.5 based on the degeneracy of the states. This departure from the theoretical ratio for the doublet implies the existence of multiple bonding environments for the Y in the films. In fact, the Y 3d peaks can be deconvoluted into two doublets using Gaussian functions. For each doublet a spin orbit splitting of 2.1 eV and peak area ratios of $I_{5/2}/I_{3/2}=1.5$ is assumed and the Full Width at Half Maximum $w$ of each doublet is permitted to vary but set equal for the 5/2 and 3/2 components ($w_{5/2}=w_{3/2}$). A good fit is obtained for width of 1.9 and 2.8 eV for the low binding energy (solid lines), and high binding energy (dashed lines) doublets. This width is higher than the ~1.7 eV resolution obtained for the current spectrometer configuration indicating that each peak includes contributions from two or more bonding states.

The existence of multiple bonding environments is corroborated by the C 1s and O 1s peaks. The C 1s region (Fig. 2b) shows a broad peak at 285 eV with a high binding energy tail and a well-resolved peak at 290.0 eV. The peak at 285 is nominally assigned to adventitious carbon and C–H bonds but the high binding energy tail may include contributions from other species. Several C–O containing species have binding energies in the specific region and a peak deconvolution using Gaussian peaks of fixed width (1.7 eV) was accomplished by including peaks at 286.5 eV (*C*–O–H, *C*–O–C), 288.0 eV (*C*=O), 289.0 eV (O–*C*=O), 290.3 eV ($CO_3$) in addition to the adventitious carbon peak at 285 eV and a small broad ($w$~2.6 eV) unassigned peak at 292.6 eV [32]. All these carbon-oxygen containing species will be referred to here as carbonates.

The O1s peak at 531.9 eV (Fig. 2c) is broad and shifted by 1.9 eV from the nominal position for the O1s peak in $Y_2O_3$ at 530 eV [22]. The location and width of the peak is compatible with the presence of hydroxylated sites and carbon containing impurities and has been deconvoluted using Gaussian peak shapes of fixed width (1.7 eV) centered at 530 eV ($Y_2O_3$), 531.7 eV (Y–OH), 532.2 eV (C=*O*, O–C=*O*), 532.8 eV (C–*O*–H, C–*O*–C), and 533.7 eV (C–*O*–C=O) [30–32].

### 3.2. Y(tmhd)$_3$ and di-tert-amyl peroxide

Fig. 2(d–f) shows the high-resolution, background corrected XPS spectra for Y 3d (Fig. 2d), C 1s (Fig. 2e), and O 1s (Fig. 2f) core electrons for $Y_2O_3$ films deposited using Y(tmhd)$_3$ and di-tert-amyl peroxide, at 90 °C, 15.86 MPa. Elemental analysis of the XPS data yields an O to Y ratio higher than the 1.5 expected for stoichiometric $Y_2O_3$ indicating the presence of excess O in the films. The Y $3d_{5/2}$ and $3d_{3/2}$ peaks for the as-deposited film are located at 158.7 eV and 160.7 eV, respectively, which are 1.9 eV higher than those reported for $Y_2O_3$ [18]. The peak height ratio for the Y $3d_{5/2}$ to $3d_{3/2}$ peaks is 1.26, smaller than the theoretically expected ratio of 1.5 based on the degeneracy of the states. This departure from the theoretical ratio for the doublet implies the existence of multiple bonding environments for the Y in the films. The C 1s spectrum exhibits an asymmetric peak at 285.0 eV and a secondary peak at 290.0 eV, respectively. A broad O 1s peak is centered at 532.0 eV. The Y3d, C1s and O1s peaks were deconvoluted using a procedure similar to that of Section (3.1), although the relative concentration of the contaminating species is different than that obtained for the tert-butyl peroxide. This difference will be examined further in the discussion section.

### 3.3. Y(tmhd)$_3$ and hydrogen peroxide

Fig. 2(g–i) shows the high-resolution, background corrected XPS spectra for Y 3d (Fig. 2g), C 1s (Fig. 2h), and O 1s (Fig. 2i) core electrons for $Y_2O_3$ films deposited from the reaction of the Y (tmhd)$_3$ precursor with a 30% aqueous hydrogen peroxide solution at 130 °C and 22.75 MPa, similar to earlier reported work [17]. Elemental analysis of the XPS data yields an O to Y ratio higher than the 1.5 expected for stoichiometric $Y_2O_3$ indicating the presence of excess O in the films. The binding energies for the Y $3d_{5/2}$ and $3d_{3/2}$ peaks are 158.5 eV and 160.5 eV respectively, which are slightly lower than those of the Y-containing films deposited with organic peroxide but still higher than the reported values for $Y_2O_3$ film. The peak height ratio for the Y $3d_{5/2}$ to $3d_{3/2}$ peaks is 1.03, smaller than the theoretically expected ratio of 1.5 based on the degeneracy of the states. This departure from the theoretical ratio for the doublet implies the existence of multiple bonding environments for the Y in the films. The C 1s spectrum exhibits an asymmetric peak at 285.0 eV and a secondary peak at 290.0 eV, respectively. The O 1s spectrum exhibits a broad peak at 532.0 eV. The Y 3d, C 1s, and O 1s peaks were deconvoluted using a procedure similar to that of Section (3.1), although the relative concentration of the contaminating species is different than that obtained for the other films. This difference will be examined further in the discussion section.

### 3.4. FTIR and AFM analysis of the films

Fig. 3(a) and (b) shows the mid- and far-infrared spectra for as-deposited and annealed $Y_2O_3$ films deposited from Y(tmhd)$_3$ and tert-butyl peroxide at similar conditions to the film in Section (3.1) above. Anneals were performed in Ar for 2 min at 400–700 °C. For the as-deposited film, the infrared spectrum exhibits a small broad band at 400–600 $cm^{-1}$, and well-resolved peaks at ~1100, 1200–1800 $cm^{-1}$ and 2800–3050 $cm^{-1}$. The vibrations associated with the $Y_2O_3$ modes usually appear in the far IR region and the broad feature at 400–600 $cm^{-1}$ is the high wavenumber tail of that spectrum [7,33]. The sharp feature at 1100 $cm^{-1}$ originates from the native oxide

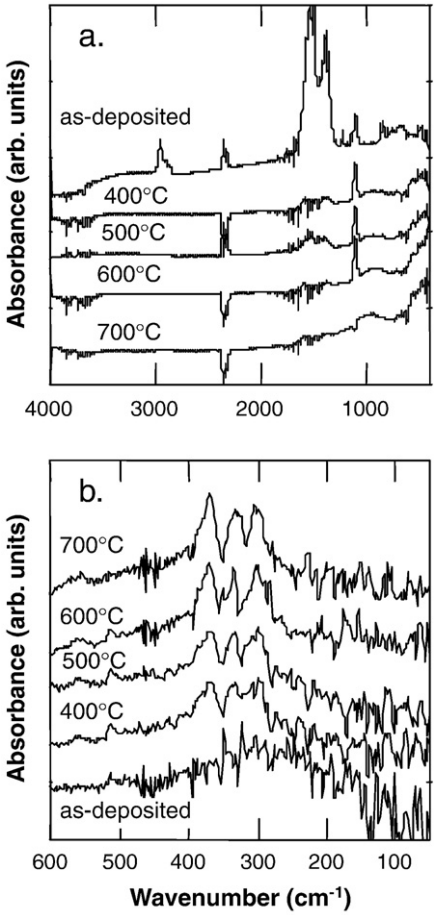


Fig. 3. (a) Mid- and (b) Far-infrared spectra for the as-deposited and annealed yttrium oxide films. The film was deposited from $Y(tmhd)_3$ and tert-butyl peroxide at 80 °C, 14.48 MPa and annealed at 400–700 °C in Ar for 2 min.

present on the Si substrates. The strong well-resolved peaks in the range of 1200–1800 $cm^{-1}$ are associated with absorptions from different carbonate species [31,27], which corroborates the XPS results. The peaks at 2800–3050 $cm^{-1}$ are attributed to the presence of C–H bonding in the film. Additionally, the weak O–H stretching modes at 3000–3600 $cm^{-1}$ result from $H_2O$ molecules adsorbed in the film and surface H-bonded OH species. After a very mild anneal at 400 °C for 2 min in Ar the infrared signatures of the O–H stretching modes and the C–H modes disappear, and the signature of the carbonate species is significantly reduced. A similar anneal at 700 °C results in almost the complete removal of the carbonate species.

The far-infrared spectrum of the as-deposited $Y_2O_3$ films shown on Fig. 3(b) displays a broad band without any significant structure between 50 and 600 $cm^{-1}$. After the high temperature anneals three clearly distinguished peaks at ~370, ~332, and ~302 $cm^{-1}$ become evident and their intensity increases with temperature. These peaks are assigned to the Y–O–Y stretching modes in $Y_2O_3$ [34].

The surface morphology of as-deposited and annealed films is analyzed by AFM and surface scans are shown in Fig. 4. Fig. 4 shows the AFM images for a 54 nm yttrium oxide film from $Y(tmhd)_3$ and tert-butyl peroxide at 80 °C, 14.48 MPa after a 1 min post deposition acetone wash (Fig. 4a) and after anneals at 400 °C (Fig. 4b) and 700 °C (Fig. 4c) in Ar for 2 min. The surface of the as-deposited film is fairly smooth with root-mean-square (RMS) roughness of 1.3 nm or ~2.4% of the film thickness. After the 400 °C anneal the film surface morphology becomes smoother with RMS roughness of 0.6 nm and further anneals up to 700 °C do not change the RMS roughness of the surface, however, the onset of island formation is observed.

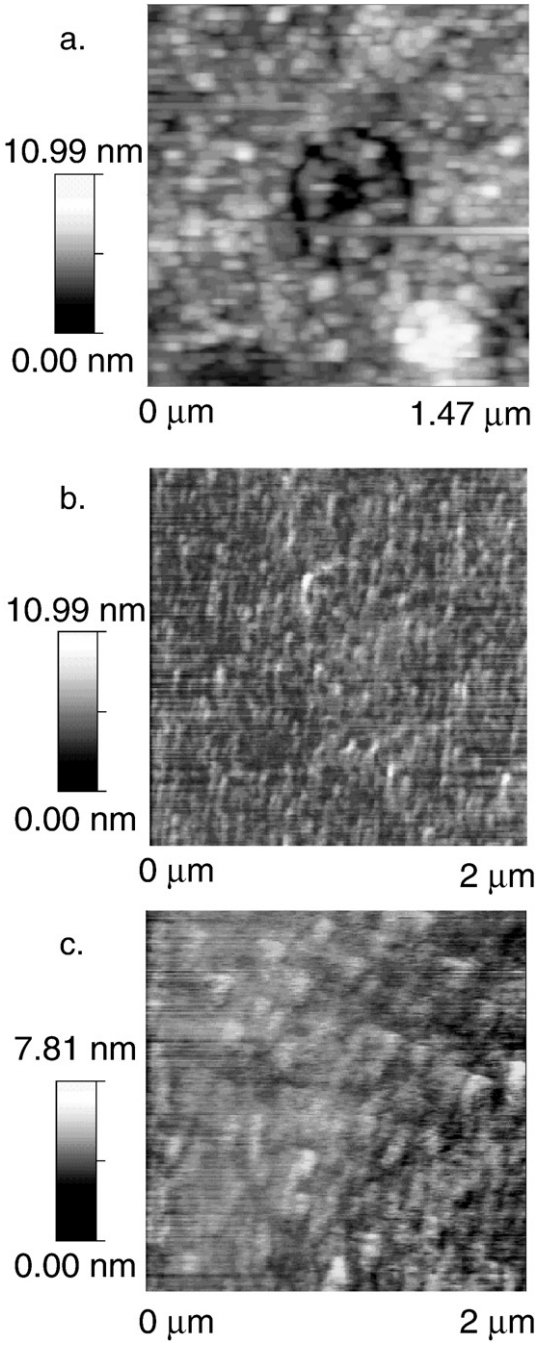


Fig. 4. AFM images for a 54.0 nm yttrium oxide film deposited from $Y(tmhd)_3$ and tert-butyl peroxide at 80 °C, 14.48 MPa and washed in acetone for 1 min post deposition (a) as-deposited and washed (b) annealed at 400 °C in Ar for 2 min and (c) annealed at 700 °C in Ar for 2 min.

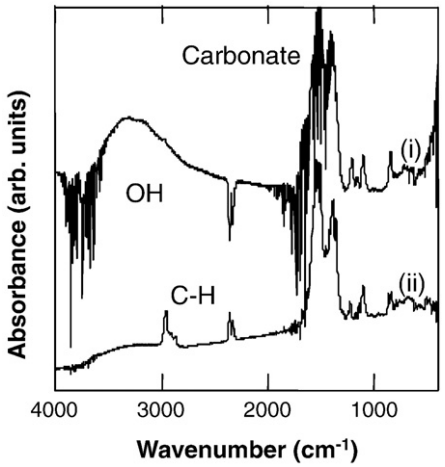


Fig. 5. Scaled IR spectrum for yttrium oxide films deposited from $Y(tmhd)_3$ with hydrogen peroxide at 130 °C (Curve i), and with tert-butyl peroxide at 80 °C (Curve ii).

Fig. 5 shows the infrared spectrum for the Y-based film deposited from hydrogen peroxide (spectrum (i)). The spectrum shows features compatible with OH (3000–3600 $cm^{-1}$) and Y–O (400–600 $cm^{-1}$) bonding in the film. The peaks at 1200–1700 $cm^{-1}$ are attributed to the presence of carbonate species in the film. For comparison, the infrared spectrum for the $Y_2O_3$ film deposited from tert-butyl peroxide is also included in Fig. 5 (spectrum (ii)). Both spectra were taken immediately after film deposition minimizing the sample exposure to the ambient. Because transmission FTIR is a bulk sensitive technique fair conclusions regarding the relative impurity concentrations can be made only if the spectra are normalized to the film thickness. SE measurements indicated that film (i) had a thickness of 20±1 nm and film (ii) had a thickness of 54±2 nm. The measured spectrum for sample (ii) was then scaled by the ratio of the two film thicknesses (20/54=0.37). As seen from the graph, the film deposited from tert-butyl peroxide exhibits weaker OH stretching mode than that from hydrogen peroxide. However, it is also observed that both hydrogen and tert-butyl peroxide deposited films exhibit similar carbonate contents.

## 4. Discussion

In this work we demonstrate a low temperature (<100 °C) synthetic approach for the deposition of $Y_2O_3$ films using the reaction of metal organic precursors with organic peroxides. The main idea behind this work is that supercritical carbon dioxide can be used as a delivery medium for the reactants and for the removal of the reaction byproducts. To accomplish that, the reactants should exhibit good solubility and this is the case for the precursor and the two organic peroxides used. The precursor solubility is easily monitored through the cell view port because of its intense orange color. Similarly, the organic peroxides preloaded in the thimble are observed to dissolve completely in the supercritical phase. Both tert-butyl peroxide and di-tert-amyl peroxides have been used for the oxidation reactions in a variety of environments [35–37], and in this work will be used for the deposition of inorganic thin films.

In a vacuum-based thermal Metal Organic Chemical Vapor Deposition (MOCVD) process, the sequence of events for film formation includes initially the adsorption and decomposition of the metal organic precursor on the heated surface. Subsequently, the organic precursor fragments react with the second reagent to form volatile products whose desorption from the surface is aided by the high surface temperature and reduced pressure in the chamber. For the approach discussed in this article the mechanism appears to be slightly different because at the low process temperature used the $Y(tmhd)_3$ precursor is fairly stable. In fact, test-runs performed in the absence of the oxygen source did not result in film formation in the temperature range of interest. It appears that decomposition of the peroxide is the reaction initiator. The thermal decomposition of dialkyl peroxides such as the ones we have used in this work have been studied extensively [38,39]. The main decomposition product of tert-butyl peroxide is the very reactive t-butoxyl radical (t-BuO*) that is known to act as an oxidizer [36]. In the $Y(tmhd)_3$ precursor the Y central atom is bonded to 3 O atoms (see Fig. 1(b)) so abstraction of an oxygen atoms is not required for the formation of $Y_2O_3$. The Y atoms are already oxidized in the $Y^{3+}$ state and removal of the undesired ligands is all that is required for film formation. As a result we propose the following reaction scheme: initially the peroxide decomposes on the cell surfaces including the substrate yielding the t-butoxyl radical as the main reactive product. Then the radicals react with the metal organic precursor leading to fragmentation. Since the precursor solubility in sc $CO_2$ is determined by the solubility of the ligands it is expected that the precursor decomposition byproducts are soluble in the supercritical phase and as such will be removed from the surface. In many ways this process resembles a plasma enhanced process where the radicals enhance the deposition rate by contributing to the precursor decomposition.

Both peroxides are known to decompose very slightly at temperatures around 100 °C in a variety of organic solvents [37,38,40]. However, although there is no data for the decomposition of the peroxides in supercritical carbon dioxide, it is well established that the presence of a supercritical medium may affect the reaction kinetics significantly and as a result may enhance the decomposition under the conditions used [41,42]. Most probably, the reaction takes place both in the supercritical phase and on the surface. However, the films are washed in a sonic bath upon removal from the cell to remove the loose precipitation byproducts of the supercritical phase reaction, and the sticky tape test performed on some of the washed samples indicated that the films are well adhered to the substrate. The composition and bonding environment for the Y atom is similar for both organic peroxides, a rather anticipated result since the chemical structure of both peroxides is very similar with only a minor difference in the hydrocarbon ligands.

In earlier work we demonstrated the use of hydrogen peroxide as an oxidizer for thin film formation and it has been used also in the course of this work [17]. Hydrogen peroxide

exhibits very poor solubility in $scCO_2$ due to its high polarity, but decomposes readily at the reaction temperatures. The hydroxyl product of that decomposition is probably responsible for the subsequent surface reaction. The major disadvantage of the use of hydrogen peroxide in this context is the incorporation of large amounts of $H_2O$ in the films. Predictably, the OH content in the films produced with the organic peroxide is significantly lower than for those using the hydrogen peroxide. Also by comparison the film formation temperature was higher for $H_2O_2$ than the organic peroxides.

Based on the IR data we can conclude that the as-deposited films are amorphous. The concurrent decrease in the intensity of the carbonate and OH content in the film and the enhancement of the intensity in the Y–O–Y stretching modes can be interpreted in the terms of the removal of hydroxyl and carbonate groups from the films, oxidation of the dangling bonds and formation of crystallites.

A sometimes undesirable by-product of the reaction of carbon dioxide with $H_2O$ on metal oxide powders is the formation of carbonate type bonding which is observed when both organic and inorganic peroxides were used. Group III-based materials including $Y_2O_3$ are fairly hygroscopic, and readily absorb moisture from the ambient producing Y–OH bonds that react further with atmospheric $CO_2$ to produce carbonate species [27–29]. The presence of these species was verified for all samples examined in this work. The Coleman-grade carbon dioxide used in this work is reported to contain 10 ppm of moisture which in the elevated reaction pressure constitutes a very significant background. As a result, it is very hard to distinguish how much of the observed carbonate products is due to reactions in the high pressure cell and how much is due to reactions after ambient exposure of the samples. The three samples examined by XPS in this article have different air exposure histories ranging from a few days to a few weeks and as a result, the relative concentration of the various carbonate species detected in the films is different.

For the films formed using the organic peroxides the IR spectra reveal the existence of C–H bonding in the films. This is probably due to incomplete removal and/or trapping of ligands in the bulk of the film. Carbon contamination in the films is fairly common in some MOCVD processes [43] and it appears to be somewhat problematic in this approach as well. Mild anneals of the film remove the IR signature of these contaminating species. However, it must be noted, that the films examined in this article were formed in a static environment that exposes the surface to an ever increasing concentration of impurities that may be incorporated in the film structure. We expect that a continuous flow approach, similar to vacuum MOCVD processes, will improve at least partially on that issue.

The AFM data show that the film surface after a one minute acetone rinse in the sonic bath removes all loose particles from the surface, leaving behind a fairly smooth film. For the film deposited using tert-butyl peroxide the AFM data indicated an RMS roughness of 1.3 nm which is less than 3% of the film thickness (54 nm) as measured by spectroscopic ellipsometry. Inert anneal of the film for 2 min at 400 °C result in smoother surface profile with an RMS roughness of 0.6 nm. Anneals at higher temperature do not affect the film roughness but the formation of islands that coincides with the onset of crystallization is observed.

## 5. Conclusions

In this work we have demonstrated the deposition of Y-containing films from the reaction of metal organic precursor with organic peroxides in supercritical $CO_2$ solutions. The XPS and FTIR results indicate that the deposited films contain Y in a variety of bonding environments including oxide, hydroxide, and carbonate. The formation of carbonate species is probably due to reactions both during film formation and after post deposition exposure to the ambient. High temperature anneals effectively remove the OH, C–H and carbonate species from the deposited films. The low deposition temperature (<130 °C) achieved in this chemical approach is significantly lower than the 350–580 °C substrate temperature used in PECVD and CVD [7,9] and somewhat lower than the 150–280 °C required for thermal ALD [12]. This technique may provide a feasible way to deposit Y-based coatings on temperature sensitive materials but the enhanced levels of bonded carbon detected in the films may make application problematic in cases where high film purity is desirable.

## Acknowledgments

Financial support from a Nanoscale Exploratory Research award from NSF (grant: CBET-0506690) and from the UMBC ADVANCE Institutional Transformation Award (grant: NSF-0244880) is gratefully acknowledged.

## References

[1] M. Swarnalatha, A.F. Stewart, A.H. Guenther, C.K. Carniglia, Appl. Phys., A Mater. Sci. Process. 54 (1992) 533.
[2] E. Masetti, A. Piegari, A. Tirabassi, SPIE Conf. Proc. 1270 (1990) 125.
[3] G. Atanassov, R. Thielsch, D. Popov, Thin Solid Films 223 (1993) 288.
[4] G.D. Wilk, R.M. Wallace, J.M. Anthony, J. Appl. Phys. 89 (2001) 5243.
[5] A.I. Kingon, J.-P. Maria, S.K. Streiffer, Nature 406 (2000) 1032.
[6] G.A. Hirata, J. McKittrick, M. Avalos-Borja, J.M. Siqueiros, D. Devlin, Appl. Surf. Sci. 113/114 (1997) 509.
[7] R.N. Sharma, A.C. Rastogi, J. Appl. Phys. 74 (1993) 6691.
[8] V.V. Bakovets, T.M. Levashova, V.T. Ratushnyak, L.F. Bakhturova, Inorg. Mater. 38 (2002) 371.
[9] D. Niu, R.W. Ashcraft, Z. Chen, S. Stemmer, G.N. Parsons, J. Electrochem. Soc. 150 (2003) F102.
[10] H. Fukumoto, T. Imura, Y. Osaka, Appl. Phys. Lett. 55 (1989) 360.
[11] J.C. Vyas, G.P. Kothiyal, K.P. Muthe, D.P. Gandhi, A.K. Debnath, S.C. Sabharwal, M.K. Gupta, J. Cryst. Growth 130 (1993) 59.
[12] P. de Rouffignac, J. Park, R.G. Gordon, Chem. Mater. 17 (2005) 4808.
[13] M. Gurvitch, L. Manchanda, J.M. Gibson, Appl. Phys. Lett. 51 (1987) 919.
[14] M.B. Korzenski, P.h. Lecoeur, B. Mercey, D. Chippaux, B. Raveau, R. Desfeux, Chem. Mater. 12 (10) (2000) 3139.
[15] G.L. Weibel, C.K. Ober, Microelectron. Eng. 65 (2003) 145.
[16] N. Kawakami, Y. Fukumoto, T. Kinoshita, K. Suzuki, K. Inoue, Jpn. J. Appl. Phys. 39 (2000) L182.
[17] T. Gougousi, D. Barua, E.D. Young, G.N. Parsons, Chem. Mater. 17 (2005) 5093.

[18] J.M. Blackburn, D.P. Long, A. Cabanas, J.J. Watkins, Science 294 (2001) 141.
[19] R.C. Reid, J.M. Prausnitz, B.E. Poling, The Properties of Gases and Liquids, 4th ed.McGraw-Hill, New York, 1987.
[20] M. McHugh, V.J. Krukonis, Supercritical Fluid Extraction, Butterworth-Heinemann, Boston, 1994.
[21] R. Baptist, A. Pellissier, G. Chauvet, Solid State Commun. 68 (1988) 555.
[22] Y. Uwamino, Y. Ishizuka, H. Yamatera, J. Electron Spectrosc. Relat. Phenom. 34 (1984) 67.
[23] J.J. Chambers, G.N. Parsons, J. Appl. Phys. 90 (2001) 918.
[24] D. Niu, R.W. Ashcraft, G.N. Parsons, Appl. Phys. Lett. 80 (2002) 3575.
[25] Y. Kuroda, H. Hamano, T. Mori, Y. Yoshikawa, M. Nagao, Langmuir 16 (2000) 6937.
[26] M.D. Ulrich, J.E. Rowe, D. Niu, G.N. Parsons, J. Vac. Sci. Technol., B 21 (2003) 1792.
[27] T. Gougousi, D. Niu, R.W. Ashcraft, G.N. Parsons, Appl. Phys. Lett. 83 (2003) 3543.
[28] M.P. Rosynek, D.T. Magnuson, J. Catal. 46 (1977) 402.
[29] S. Bernal, J.A. Diaz, R. Garcia, J.M. Rodriguez-Izquierdo, J. Mater. Sci. 20 (1985) 537.
[30] M. Ronay, E.-E. Latta, Phys. Rev., B 27 (1983) 1605.
[31] T. Sugama, J. Sol-Gel Sci. Technol. 12 (1998) 35.
[32] B.D. Ratner, D.G. Castner, in: J.C. Vickerman (Ed.), Surface Analysis: The Principle Techniques, Wiley, West Sussex, 1997, p. 51.
[33] T. Tsutsumi, Jpn. J. Appl. Phys. 9 (1970) 735.
[34] Y. Nigara, M. Ishigame, T. Sakura, J. Phys. Soc. Jpn. 30 (1971) 453.
[35] M. Vazylev, D. Sloboda-Rozner, A. Haimov, G. Maayan, R. Neumann, Top. Catal. B 34 (2005) 93.
[36] B. Mihaljevic, D. Razem, Radiat. Phys. Chem. 67 (2003) 269.
[37] J.C. Oxley, J.L. Smith, E. Rogers, W. Ye, A.A. Aradi, T.J. Henly, Energy Fuels 14 (2000) 1252.
[38] J.H. Raley, F.F. Rust, W.E. Vaughan, J. Am. Chem. Soc. 70 (1948) 88.
[39] L. Batt, S.W. Benson, J. Chem. Phys. 36 (1962) 985.
[40] P. Skrdla, Int. J. Chem. Kinet. 36 (2004) 386.
[41] K.P. Johnston, C. Haynes, AIChE J. 33 (1987) 2017.
[42] P.E. Savage, S. Gopalan, T.I. Mizan, C.J. Martino, E.E. Brock, AIChE J. 41 (1995) 1723.
[43] B.-O. Cho, S. Lao, J.P. Chang, J. Appl. Phys. 93 (2003) 9345.